ACS OMEGA

http://pubs.acs.org/journal/acsodf

Article

Interfacial Behavior and Dechlorination Reaction of Water Droplet Impact on a Heated Extracted Titanium Tailing Surface

Yan Zhao, Liangying Wen,* Bo Liu, Li Su, Meilong Hu, Shengfu Zhang, and Jianxin Wang

Cite This: *ACS Omega* 2023, 8, 19433−19442

Read Online

ACCESS | Metrics & More | Article Recommendations

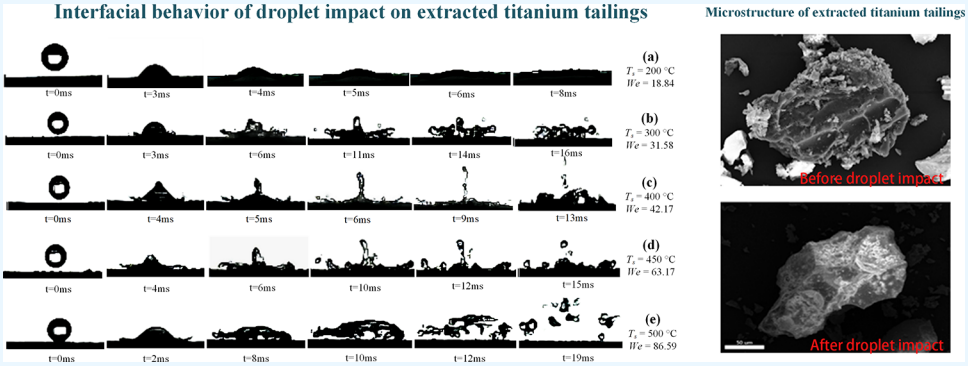

ABSTRACT: The interfacial behaviors of the droplet impact on a heated extracted titanium tailing surface are studied experimentally. The effects of surface temperatures and Weber numbers on the droplet spreading characteristics are examined. The factors affecting the mass fraction and dechlorination ratio of extracted titanium tailings under the action of interfacial behavior have been researched by thermogravimetric analysis. The compositions and microstructures of extracted titanium tailings are characterized using X-ray fluorescence spectroscopy and scanning electron microscopy-energy dispersive spectroscopy (SEM-EDS). The interfacial behaviors on the extracted titanium tailing surface are classified into four regimes, i.e., boiling-induced break-up, advancing recoiling, splash with a continuous liquid film, and splash with a broken film. The maximum spreading factors increase with the surface temperature and the Weber number. It is found that the surface temperature has a dominant influence on the spreading factors and interfacial effect, further affecting its chlorination reaction. SEM-EDS analysis revealed that the extracted titanium tailing particles are irregular shaped. There are some fine pores on the surface after the reaction. The main concentrations are Si, Al, and Ca oxides with a certain amount of C elements. The findings of this research provide a new pathway to utilize the extracted titanium tailings comprehensively.

1. INTRODUCTION

Vanadium−titanium-bearing magnetite is a valuable raw material, containing the metallic elements of titanium and vanadium. The titanium resources of the V−Ti magnetite account for 35.17% of the world's titanium reserves.[1,2] The V−Ti magnetite concentrate contains more than 50% titanium resource of China total reserves. Almost all the titanium remains in the slag, forming a titanium-bearing blast furnace slag (TBBFS) in the blast furnace process.[3,4] For a long time, the related enterprises and research institutes did not find a proper method to treat the TBBFS, resulting in plenty of solid waste.[5] It occupies the farmland, wastes titanium resources, and pollutes the environment.[6] Therefore, it is necessary to develop a practical approach to utilize the titanium resources of the TBBFS comprehensively. The Pangang Group conducted the "high-temperature carbonization and low-temperature chlorination processes" to treat TBBFS.[7] The TiO_2 is carbonized to TiC in TBBFS under high temperatures.[8] Then, the carbonized slag is cooled and crushed as a raw material for chlorination, and the TiC is converted to $TiCl_4$ in the chlorination furnace.[9] This processing method has an advantage over recovering titanium resources from TBBFS. However, the extracted titanium tailings account for 80% of TBBFS after treatment.[10] The extracted titanium tailings that account for above 5% chloride ions cannot be directly utilized.[11] Accordingly, investigating efficient and low-cost dechlorination is imperative to realize the harmless and large-scale comprehensive utilization of tailings.

Received: January 30, 2023
Accepted: April 25, 2023
Published: May 24, 2023

The extracted titanium tailing is a unique residue in the southwest region of China. There are few studies on removing chloride ions from titanium extraction tailings. Conventional dechlorination methods of extracted titanium tailings are as follows:[12,13] "water washing", "calcination with a slight addition of water", "washing-calcination", and "multi-stage washing calcination". These five approaches are feasible in practical applications, but most expose some problems, such as high cost, low efficiency, and environmental pollution.

Experimental investigations of the impact process of a droplet on a heated surface began in the 1960s. Numerous research studies have mainly been made on the droplet impact on conventional metal surfaces (e.g., stainless steel, aluminum, etc.).[14,15] The droplet impact behavior on the porous ceramic surface have also been explored.[16] Many investigations show that Weber number and surface temperature have essential effects on droplet interfacial behaviors.[17−20] The Weber number represents the ratio of inertia force and the surface tension and is formulated as

$$We = \rho v_0^2 D_0/\gamma \quad (1)$$

where ρ and γ are the density and surface tension of the liquid and v_0 and D_0 are the initial velocity and diameter of the droplet, respectively. However, few studies have looked into the interfacial behaviors of the droplet impact on an extracted titanium tailing surface. Tran et al.[21] investigated a liquid droplet impact on heated surfaces above the boiling point. The impact behaviors were observed when the droplet contacted the surface at variable conditions of the Weber number and surface temperatures. They also built the scaling law of the maximum spreading factor with the Weber number of the droplets. Jadidbonab et al.[22] experimentally studied the impact process of diesel-fuel droplets on a heated solid particle. It concluded that the dimensionless maximum spreading increases with the Weber number but decreases with the particle temperature. Moita and Moreira[23] explored the impact behaviors on the heated surface in the millimeter range of several kinds of liquid droplets, such as water, isooctane, and ethanol. Liang et al.[24] studied the impingement of a liquid droplet on cylindrical surfaces with different curvatures. Then, the phenomena of rebound, spread, and splash of the droplet occur in succession with the increase of impact velocity for the curvature ratio less than 0.5. Quéré[25] investigated the interfacial behaviors of droplet impact on the hot solid surface and quantitatively analyzed the effects of the Weber number and surface temperature on the residence time and the spreading diameter of droplets. Bain et al.[26] conducted droplet impact experiments in a Petri dish atop a heater/stirrer with a surface temperature between 400 and 500 °C. It was shown that chemical reactions could be accelerated in levitated droplets, and it concluded that interfacial effects contribute to acceleration. Abdelaziz et al.[27] employed a levitated Leidenfrost droplet of aqueous solution on overheated substrates to fabricate metal nanoparticles. Adda-Bedia et al.[28] conducted inverse Leidenfrost experiments by levitating droplets on a liquid nitrogen bath. Above all, proper control of droplet impingement on these surfaces is favorable for the desired chemical processes. Knowledge of droplet impact behaviors and spreading characteristics is helpful in improving their performance.

In our previous research,[29,30] we investigated the macroscopic behaviors of droplet impingement on the tailing surface by CFD simulations, and a few experiments were performed to verify the simulation results. However, the microstructure and elemental distribution of the tailings surface after droplet impact are not involved. As expected, the interfacial effect is accompanied by the hydrodynamic behavior of water droplet impact on the heated surfaces. In the present study, the effect of surface temperature and Weber number on the interfacial behaviors and spreading characteristics of the droplet impact on the heated extracted titanium tailing surface is explored in detail using a high-speed camera. The influence of temperature on the dechlorination reaction of extracted titanium tailings is studied in depth under the action of interfacial effect. The element distributions, morphology characterizations, and existing states of extracted titanium tailings after the dechlorination reaction are explored. The findings will provide a technical basis for extracted titanium tailings of harmless treatment and resource reuse as well as improve thermal engineering.

2. EXPERIMENTAL SECTION

2.1. Materials and Apparatus. Figure 1 illustrates a diagram of the present experimental apparatus for observing interfacial behaviors and detecting reactor mass. The extracted titanium tailing used in this experiment was supplied by the Pangang Group (Panzhihua region, Sichuan province, China). Table 1 shows the chemical contents and element types of extracted titanium tailings. Extracted titanium tailings are prepared to form a cylindrical sample with a radius of the cross section of 30 mm and a height of 10 mm. The standard contact angle was measured by the KRUSS DSA30 at room temperature, the contact angle of a water droplet on the surface was 112.6°, and the surface was hydrophobic. The surface roughness was measured by the Mitutoyo SJ-210 surface roughness meter. The mean surface roughness (Ra) was 1.6 μm. The cylindrical sample in the reactor was heated by a heating system with a temperature controller. A mobile K-type thermocouple was used in measuring the surface temperature range up to 500 °C. A needle with different inner diameters (0.3, 0.5, and 0.8 mm) was connected to a syringe pump. The syringe pump was used to feed water with a volume rate of 1 mL/min. The shape of the falling droplet was not perfectly spherical under the influence of gravity. The equivalent diameter of the droplet was obtained by eq 1.[31]

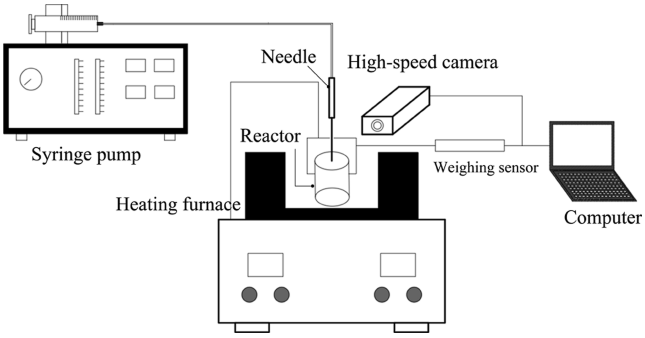

Figure 1. Schematic of the experimental apparatus.

$$D_0 = (D_v D_h^2)^{1/3} \quad (2)$$

where the droplet of the vertical diameter D_v and the horizontal diameter D_h can be measured.

https://doi.org/10.1021/acsomega.3c00612
ACS Omega 2023, 8, 19433−19442

Table 1. Components of Extracted Titanium Tailings[a]

components	TiC	CaO	MgO	SiO_2	TiO_2	Al_2O_3	MnO	$CaCl_2$	$MgCl_2$	$MnCl_2$	C
mass fraction	3.26	29.08	8.55	27.80	2.25	14.43	0.72	3.86	0.55	0.05	9.45

[a](%).

The average diameter of water droplets D_0 is 2.03, 2.48, and 3.04 mm. The impact velocity can be obtained by analyzing the translation distance of the droplet during 1 ms. The initial impact velocity ranges from 0.95 to 1.44 m/s, corresponding to the Weber number from 18.84 to 86.59. The impact Weber numbers of the droplet are summarized in Table 2. A water droplet generated through a needle detaches when gravity is dominant over the surface tension. The weighing sensor is used to record the mass change of the extracted titanium tailings during the roasting and droplet impact process. The weighing data are recorded on the computer.

Table 2. Droplet Impact Conditions

	ν_0 (m/s)		
D_0 (mm)	0.95	1.23	1.44
1.5	*We* = 18.84	*We* = 31.58	*We* = 43.29
2.0	*We* = 25.12	*We* = 42.17	*We* = 57.73
3.0	*We* = 37.69	*We* = 63.17	*We* = 86.59

The extracted titanium tailing was weighed 5 g and placed in the reactor. The reactor was heated in a heating furnace from room temperature to predetermined temperatures, and then, it was kept in heat preservation for 15 min. The predetermined temperatures ranged from 100 to 500 °C. After the temperature stabilization, the weight was measured in real time by a weighing sensor. The needle was adjusted to a height of 20 mm away from the tailings. The syringe pump was turned on for 5 min with a charging rate of 1 mL/min. Each experiment under different conditions was performed repeatedly at least three times.

2.2. Analysis and Characterization. The droplets' interaction with the extracted titanium tailing surface was observed by a high-speed camera (IDT Y4-S1) with a 35 mm KOWA macro lens at f/1.4 aperture, which had an image frequency of 15,000 fps at the full resolution of 256 × 128 pixels. The camera was placed horizontally, parallel to the tailing sample surface. The size of droplets was obtained by pixel analysis of the droplet images captured by the high-speed camera. The image sequences of droplet behaviors were analyzed by Image-Proplus 6.0 (Media Cybernetics Corporation, Rockville, MD, USA) software. The spreading dimension of droplets was also measured.

The chemical composition of the extracted titanium tailings was characterized by using an X-ray fluorescence spectrometer (XRF-1800, SHIMADZU, Japan). The morphology and element analysis of extracted titanium tailings were analyzed using scanning electron microscopy-energy dispersive spectroscopy (Quattro S, Thermo Fisher Scientific, Waltham, USA).

The uncertainty of the surface temperature was created by the thermocouple placement and errors in the measured temperature. The imaging pixel resolution of the high-speed camera was calculated by observing an object with a known length and measuring the length in pixels of the image. According to the error estimation of Negeed et al.,[32] the error in surface temperature was probably ±0.6 °C. The error in the pixel resolution was approximately ±0.021 μm/pixel.

3. RESULTS AND DISCUSSION

3.1. Interfacial Behaviors on the Extracted Titanium Tailing Surface. Figure 2 shows the interfacial behaviors of droplet impact on the extracted titanium tailing surface. The

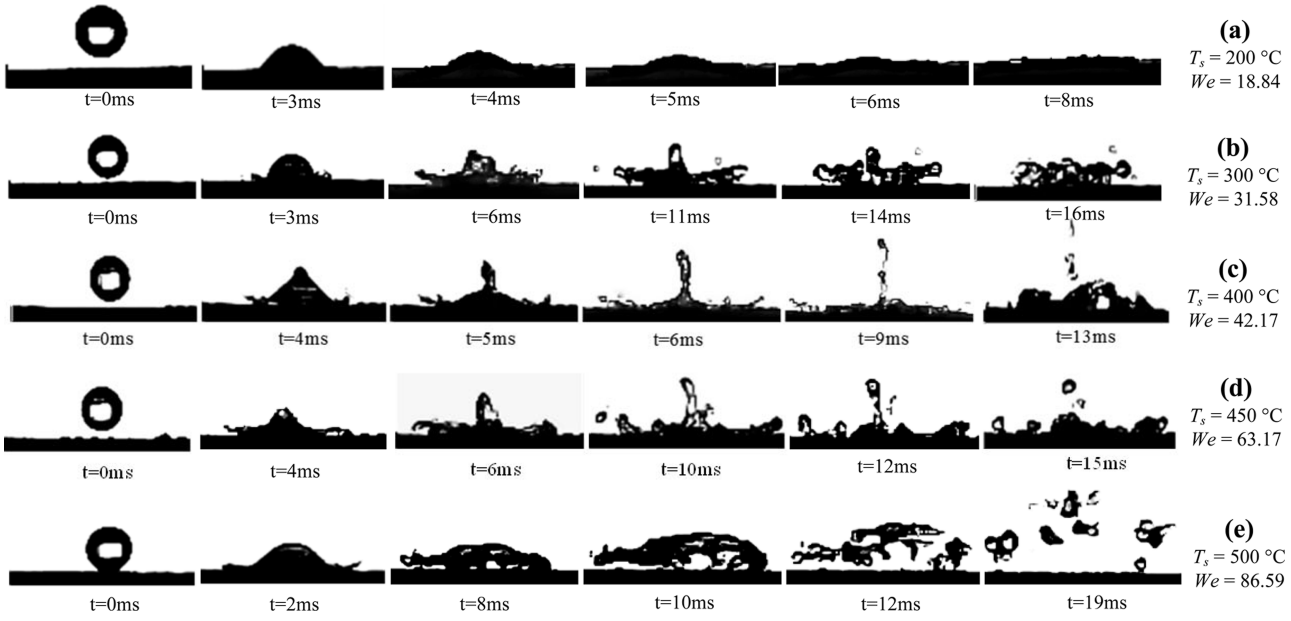

Figure 2. Impact behaviors of droplets on heated tailing surfaces: (a) T_s = 200 °C, *We* = 18.84; (b) T_s = 300 °C, *We* = 31.58; (c) T_s = 400 °C, *We* = 42.17; (d) T_s = 450 °C, *We* = 63.17; (e) T_s = 500 °C, *We* = 86.59.

https://doi.org/10.1021/acsomega.3c00612
ACS Omega 2023, 8, 19433−19442

dynamic behaviors are classified into five regimes: spread, boiling-induced break-up, advancing recoiling, splash with a continuous liquid film, and splash with a broken liquid film.

In the early stage of impact between the droplet and the tailing surface, the top half part of the droplet remains spherical at t = 3 ms, while the bottom part gradually spreads out in all directions. The gravitational potential energy of the droplet is gradually transformed into kinetic energy and a liquid film is formed after the saturation of the surface voids at 8 ms. The spreading speed of the droplet gradually decreases under the effect of surface tension. In the whole spreading process, the droplet and the tailing surface are in a state of adhesion. This regime is named as spread occurring at T_s = 200 °C and We = 18.84. Figure 2b displays the selected snapshots of a droplet impact on a heated tailing surface at a temperature of 300 °C and the Weber number of 31.58. During the initial impact process, the droplet contacts the tailing surface and spreads under the effect of inertia. At t = 11 ms, the droplet further spreads out to form a thin liquid film. The droplet gradually comes into the boiling stage due to the heat exchange between the tailing surface and the droplet. At t = 16 ms, the droplets roll on the surface under the effect of vapor pressure and the capillary effect of extracted titanium tailings. The "advancing recoiling" regime for the droplets impinging on the tailing surface occurs at T_s = 400 °C and We = 42.17, as shown in Figure 2c. The droplet spreads and reaches the maximum spreading diameter under the effect of the initial kinetic energy and then retracts to be in an equilibrium stage. As temperature rises, a reaction force generated from the vapor layer dominates over the initial kinetic energy, resulting in the appearance of a "Worthington jet"[33] at t = 5 ms. The vertical liquid jet is directed along the outer normal to the surface and moves upward at t = 13 ms. Figure 2d shows the selected snapshots of the droplet behaviors on the extracted titanium tailing surface at T_s = 450 °C and We = 63.17. During the initial impact period, the droplet has sufficient initial momentum to overcome the surface tension because of the increased Weber number. The edge of the liquid droplet moves toward the central part. Subsequently, a liquid column occurs at t = 6 ms. The droplet gradually evolves into a mountain-shaped liquid film. At t = 15 ms, several child droplets form at the rim and neck of the unstable liquid film and break up. At the same time, the central part of the liquid film remains continuous. Therefore, this regime is defined as splash with a continuous liquid film. Figure 2e shows the morphology of a droplet on the tailing surface at T_s = 500 °C and We = 86.59. As the surface temperature increases, there is more heat exchange between the tailing surface and the droplet. As a result, many air bubbles are formed at the solid−liquid interfaces. The liquid film breaks up when the droplet reaches the maximum spreading diameter, generating a few secondary droplets at t = 15 ms. These secondary droplets have relatively great kinetic energy and bounce off the surface. This regime is defined as splash with a broken liquid film.

The interfacial behaviors of the droplet impingement on the extracted titanium tailing surface are influenced by the surface temperature and Weber number. Figure 3 shows a phase map considering the present parameters. The evaporation rate is relatively low at low temperatures ($T_s \leq$ 200 °C); the spread regime is independent of the impact Weber number. When the boiling-induced break-up regime starts at the surface temperature rising over 220 °C, the initial downward momentum dominates over the reaction force from the production and

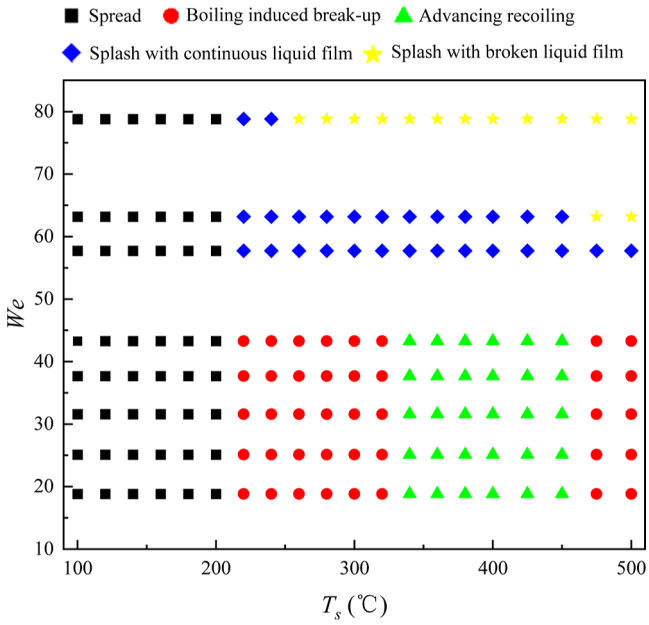

Figure 3. Regime map of the droplet impact on an extracted titanium tailing surface.

compression of a thin vapor layer. As temperature further rises (340 °C ≤ T_s ≤ 450 °C), the upward reaction force increases and overcomes the initial downward momentum, triggering the recoil phenomenon. As the surface temperature is larger than 450 °C, the evaporation rate increases and a stable vapor layer is produced, which reduces the heat transfer rate and the reaction force. Hence, the downward momentum overcomes the reaction force. The advancing recoiling phenomenon is suppressed, and the Worthington jet cannot be observed. The splash phenomenon depends on the impact Weber number and occurs at a medium Weber number (57.73≤ We < 78.8). Increasing the Weber number means increasing the kinetic energy, and the spreading liquid film becomes highly unstable across the spreading area. With a further increase in the Weber number, the inertia force is enough to overcome the surface tension of the droplet to attract the Rayleigh-Plateau instability, and the splash with the broken liquid film regime occurs ($We \geq$ 78.8 at $T_s \geq$ 260 °C). Moreover, compared with the dynamics of the droplet on the smooth surface,[34] the interfacial behaviors of the droplet on the extracted titanium tailing surface are subtly different. The main difference is that the droplet will rebound from the smooth surface at a higher temperature (i.e., steel surface with a temperature of 280−325 °C). As explained by Zhao et al.,[35] when the droplet impacts on the porous surface, the rebound phenomenon does not occur. On the one hand, this difference is mainly caused by the capillary effects of the rough tailing surface. The tailing surface absorbs much kinetic energy to resist the rebound of the droplet. On the other hand, the thermal conductivity of extracted titanium tailings is lower than that of the steel surfaces.

3.2. Spreading Characteristics. To investigate the effects of surface temperature and Weber number on the spreading characteristics of the droplet on the extracted titanium tailing surfaces, the droplet spreading factor β is formulated as

$$\beta = \frac{D_t}{D_0} \tag{3}$$

https://doi.org/10.1021/acsomega.3c00612
ACS Omega 2023, 8, 19433−19442

where D_t is the diameter of the liquid−solid interface, and D_0 is the initial droplet diameter.

Figure 4 illustrates the time evolutions of spreading factors on the extracted titanium tailing surface with different

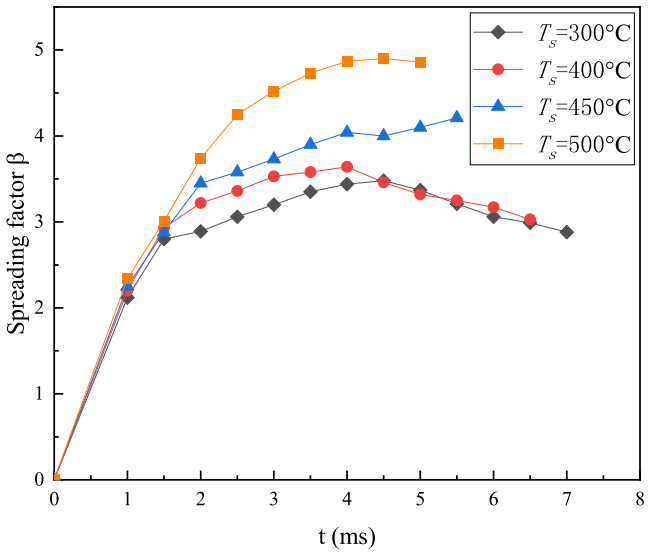

Figure 4. Spreading factors against time on the tailing surface at $We \approx 57.73$ with different surface temperatures.

temperatures. It can be seen that the maximum spreading factors become larger as the surface temperature increases. At surface temperatures $T_s \leq 400$ °C, the droplets get levitated by the vapor layer after reaching the maximum spreading diameter and retract due to the effect of surface tension. In the break-up regime at $T_s \geq 450$ °C, the air bubble occurs at the liquid−solid interfaces more fiercely, and the droplet is interrupted more frequently. As a consequence, the droplet spreads to reach the maximum spreading factor and is shattered into several secondary droplets.

The variations of the spreading factors of the droplet impact with different Weber numbers at T_s = 400 °C are shown in Figure 5. The droplet spreads faster and reaches the larger maximum spreading factor when the Weber number increases. The inertia force is dominant at the initial impact stage. Subsequently, the droplet begins retracting under the action of surface tension. The surface tension becomes larger as soon as the maximum spreading diameter is larger, leading to quick retraction of the droplet. However, when the Weber number increases to 86.9, the droplet has enough inertia to overcome the surface tension. The rupture phenomena occur after reaching the maximum spreading factor.

The maximum spreading factors obtained from the present experiments are compared with the scaling laws of the maximum spreading factors in previous research studies, as shown in Figure 6. The predicted values of Tran,[21] Clanet,[36] Wang,[37] and Liang[38] are applied for comparison. A correction to predict the maximum spreading factor β_{max} can be represented as $\beta_{max} = cWe^a$,[39] where c and a are obtained by regressing experiments data. The best analytical fit to the experimental results for the extracted titanium tailing surface is depicted in this figure, which corresponds to the following correction

$$\beta_{max} = 0.504We^{0.412} \tag{4}$$

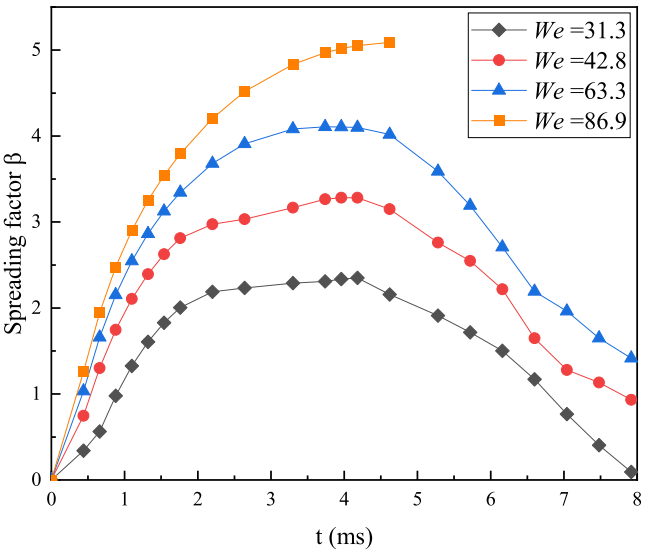

Figure 5. Spreading factors against time on the tailing surface at T_s = 400 °C with different Weber numbers.

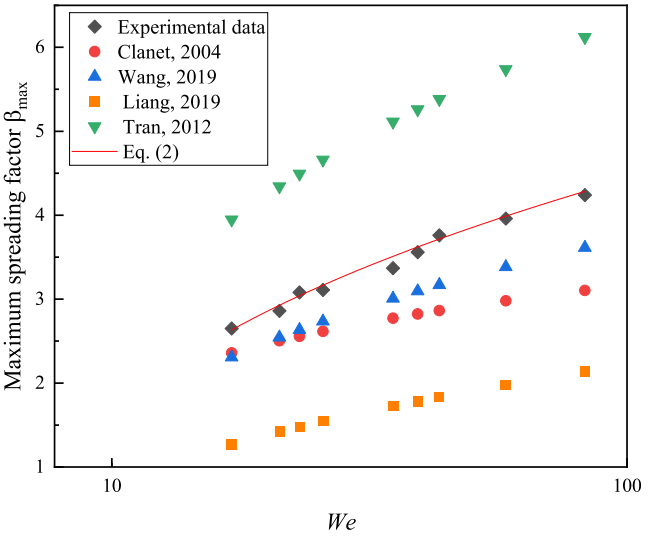

Figure 6. Effect of Weber numbers on the droplet maximum spreading factor. (The solid line represents the prediction of $\beta_{max} = 0.504We^{0.412}$ in the present study.)

The scaling laws of eq 2 are in agreement with the measured data by the experiment. The predictions of maximum spreading factors by Clanet, Liang, and Wang are below eq 2 in the present work, while the prediction of Tran is above eq 2.

In the process of the droplet impacting and spreading with the heated surface, the kinetic energy of the droplet is partially converted into surface energy and dissipated due to viscosity. The kinetic energy is zero when the droplet reaches the maximum spreading diameter. Based on the energy balance of the droplet,[40] the relationship of the maximum spread diameter of the droplet is established as

$$E_{K0} + E_{\gamma 0} = E_{\gamma max} + \Psi \tag{5}$$

The initial kinetic energy E_{K0} and surface energy $E_{\gamma 0}$ of the droplet before impingement are

$$E_{K0} = \left(\frac{1}{2}\rho v_0^2\right)\left(\frac{\pi}{6}D_0^3\right) \tag{6}$$

https://doi.org/10.1021/acsomega.3c00612
ACS Omega 2023, 8, 19433−19442

$$E_{\gamma 0} = \pi {D_0}^2 \gamma \tag{7}$$

The surface energy of the droplet reaching the maximum spreading factor $E_{\gamma max}$ is

$$E_{\gamma max} = \pi/2 {D_{max}}^2 \gamma + \pi D_{max} h \gamma \tag{8}$$

The impacting droplet is supposed to be a cylinder; the droplet height h is defined as

$$h = \frac{2{D_0}^3}{3{D_{max}}^2} \tag{9}$$

The dissipation energy Ψ of the spreading droplet is

$$\Psi = \int_0^{t_l} \int \phi \, dV \, dt \approx \phi V t_l \tag{10}$$

The dissipation function ϕ, droplet volume V, and spreading time t_l can be described as

$$\phi \sim \mu \left(\frac{v_0}{h}\right) \tag{11}$$

$$V \sim 1/4 \pi {D_{max}}^2 h \tag{12}$$

$$\frac{1}{2}\rho {v_0}^2 \sim \mu \left(\frac{v_0}{h}\right) \tag{13}$$

where μ represents liquid viscosity. Moreover, the dissipation energy Ψ of the droplet reaching the maximum spreading factor is given by

$$\Psi = C \cdot \rho {v_0}^2 D_0 {D_{max}}^2 \tag{14}$$

Eq 2 can be rewritten as

$$\frac{\pi}{12}\rho {v_0}^2 {D_0}^3 + \gamma \pi {D_0}^2 = \gamma \left(\frac{\pi}{2}{D_{max}}^2 + \pi D_{max} h\right) + C \cdot \rho {v_0}^2 D_0 {D_{max}}^2 \tag{15}$$

The constant C is set as $C = 0.00024$ based on experimental values. The scaling law between the maximum spreading factor and the Weber number of the droplet can be determined as

$$(We + 12)\left(\frac{D_{max}}{D_0}\right) - (6 + 0.0009We)\left(\frac{D_{max}}{D_0}\right)^3 - 8 = 0 \tag{16}$$

3.3. Dechlorination Experiments of Extracted Titanium Tailings. The main chloride of extracted titanium tailings is $CaCl_2$, which could react with O_2 and H_2O as follows

$$CaCl_2(s) + O_2(g) \rightarrow CaO(s) + Cl_2(g) \tag{17}$$

$$CaCl_2(s) + H_2O(l) \rightarrow CaO\,(s) + HCl(g) \tag{18}$$

$$CaCl_2(s) + H_2O(l) + O_2(g) + C(s) \rightarrow CaO(s) + HCl(g) + CO_2(g) \tag{19}$$

Figure 7 shows the weight of the extracted titanium tailings recorded by the weighing sensor in a temperature range from 300 °C to 500 °C. Note that the mass fraction of extracted titanium tailings was similar in the initial 900 s of roasting time when the surface temperature was raised from 300 to 400 °C, accompanied by a tendency of rapid decrease and then gradual stabilization. The weight loss ratio was 5−6% before water droplet impact. Further increasing the surface temperature to 500 °C, there was a significant reduction in the mass fraction of extracted titanium tailings, with a weight loss ratio of 9%. The mass fraction reduction of extracted titanium tailings during roasting was related to the reaction of chloride with O_2 to form Cl_2 during the heating process. When the water droplets impact on the extracted tailing surface at $t > 900$ s, the mass fraction slightly increases and then decreases dramatically. The reaction acceleration is apparent in extracted titanium tailings, which is associated with the interfacial behaviors of the droplets impacting on the heated surface. Moreover, the heat mass exchange between droplets and heated extracted titanium tailings is intensive. The interfacial effect resulting from thermodynamic behaviors contributes to reaction acceleration.

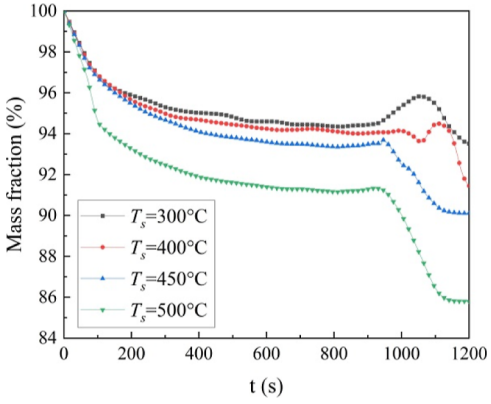

Figure 7. Mass fraction of extracted titanium tailing surface with different surface temperatures.

3.4. Elemental Composition and Microstructure of Extracted Titanium Tailings. Figure 8 shows XRF elemental analysis of extracted titanium tailings under conditions of the droplet impingement on the tailing surfaces with different temperatures (300, 400, 450, and 500 °C). The Cl concentration of extracted titanium tailings before the reaction is 5.08%. When droplets impact on the surface, the Cl concentrations of the extracted titanium tailings after the reaction are 3.27% (300 °C), 2.51% (400 °C), 2.21% (450 °C), and 1.03% (500 °C). It indicates that the Cl

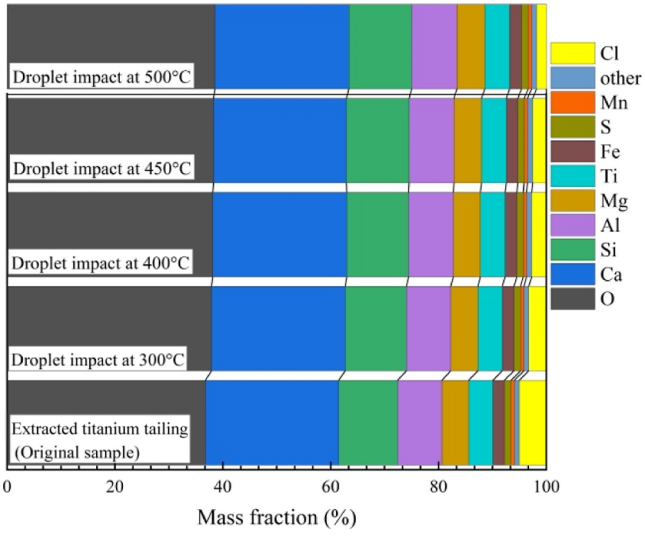

Figure 8. XRF elemental analysis results of extracted titanium tailings.

https://doi.org/10.1021/acsomega.3c00612
ACS Omega 2023, 8, 19433−19442

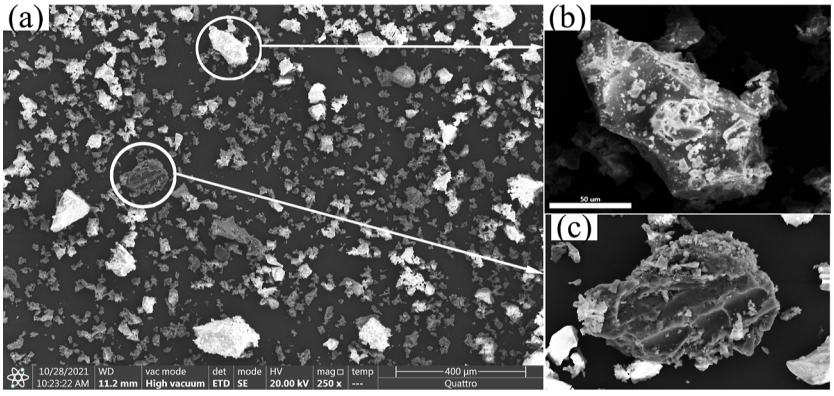

Figure 9. Morphologies of extracted titanium tailing particles before reactions [(a): SEM images; (b,c) local enlarged view of (a)].

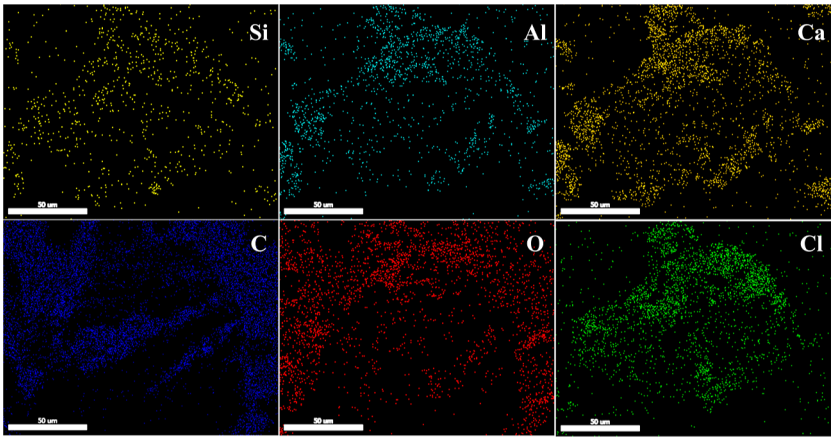

Figure 10. Element distributions on the surface of the material particles before droplet impact.

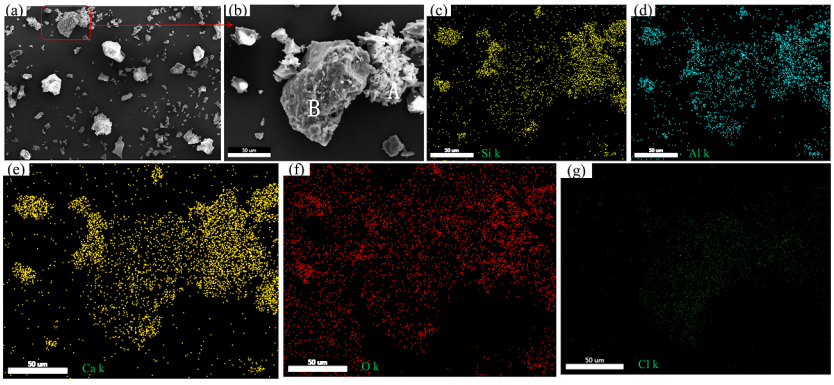

Figure 11. SEM/EDS analyses of extracted titanium tailings after reaction with the droplet impact at 300 °C. (a) Microstructure of the tailings surface; (b) local enlarged view of (a); (c) distribution of the Si element; (d) distribution of the Al element; (e) distribution of the Ca element; (f) distribution of the O element; (g) distribution of the Cl element.

concentration of the extracted titanium tailings after droplet impact gradually reduces with the increased surface temperature. Heat is a critical factor in facilitating reactions in Leidenfrost droplets and has been considered as a potential source of acceleration in the dechlorination reaction.[26] The higher the surface temperature, the more plentiful the heat exchange between the droplet and the surface. As a result, the dechlorination reaction of H_2O and $CaCl_2$ in extracted titanium tailings was accelerated at a higher temperature, and the largest element variation was observed at 500 °C. Results from the XRF analysis supported the conclusion that the mass fraction of the extracted titanium tailings decreases when the surface temperature increases, as shown in Figure 4.

The surface morphology and element distribution of extracted titanium tailings and their concentrates are observed by SEM-EDS, as shown in Figure 9. Figure 9a is the SEM image of extracted titanium tailings before the reaction. The raw particles are mainly composed of some medium bright particles and gray particles. Partial gray particles are agglomerated. Figure 9b,c shows the regional up-scaling views of Figure 9a. The shape of the particles is irregular. Most of the bright particles have sizes greater than 50 μm. Figure 10 shows the elemental distributions of the gray

https://doi.org/10.1021/acsomega.3c00612
ACS Omega 2023, 8, 19433−19442

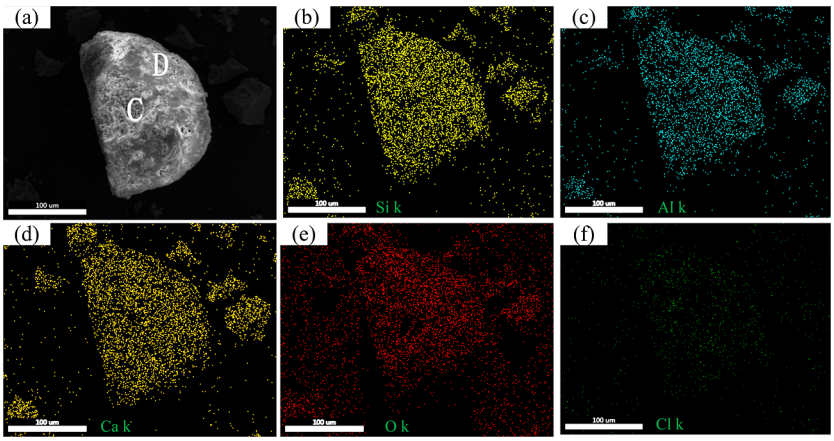

Figure 12. SEM/EDS analyses of extracted titanium tailings after reaction with the droplet impact at 400 °C. (a) Microstructure of the tailings surface; (b) distribution of the Si element; (c) distribution of the Al element; (d) distribution of the Ca element; (e) distribution of the O element; (f) distribution of the Cl element.

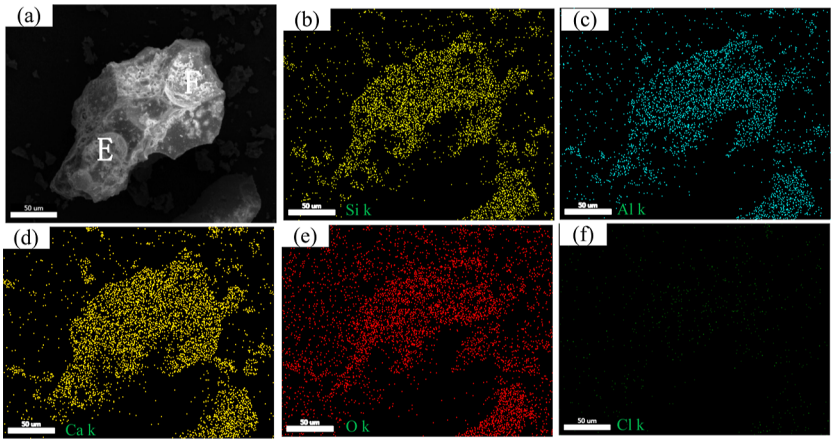

Figure 13. SEM/EDS analyses of extracted titanium tailings after reaction with the droplet impact at 500 °C. (a) Microstructure of the tailings surface; (b) distribution of the Si element; (c) distribution of the Al element; (d) distribution of the Ca element; (e) distribution of the O element; (f) distribution of the Cl element.

particles before the dechlorination reaction (Figure 9c). From the results of elemental distributions, compared with other elements, the enrichment region of the C element is independently distributed. In addition, the element distributions of Ca and Cl are in good coincidence. Accordingly, the main composition of the enrichment region is $CaCl_2$. The Si and Al oxides can also be observed from EDS analysis.

The microstructure and elemental analysis of the extracted titanium tailings after the reaction were investigated by varying different surface temperatures. The particles of most regions are loose, and partial particles agglomerate after droplet impact at T_s = 300 °C, as shown in Figure 11. Figure 12 shows that the fine pores are distributed over the surface of particles. The extracted titanium tailings are dissolved and dechlorinated after droplet impact under the interfacial effect of water vapor evaporation. Figure 13 displays the microstructure of the tailing surface after the dechlorination reaction has some concaves, and more micro-pores are distributed in the concaves. Due to the further temperature increase, the interfacial effect of droplets impacting on the extracted titanium tailings is enhanced. As a result, the dissolution dechlorination reaction is more intensive. Table 3 shows the element types and contents at specific positions on the material particles after the reaction. The contents of Cl are 2.61 and 2.89% in positions A and B at T_s = 300 °C, respectively. The contents of Cl are 1.67 and 1.71% in positions C and D at T_s = 400 °C. The contents of Cl are 0.4 and 0.81% in positions E and F at T_s = 500 °C. After the reaction, the main compositions of positions are O element with 22.83−46.78% and C element with 8.7−20.41%. It indicates that the Cl contents of the extracted titanium tailing particles gradually decrease with the increasing surface temperature, which basically agrees with the XRF elemental analysis in Figure 8. From the elemental analysis results, the primary concentrations of extracted titanium tailing particles are oxides of Si, Al, and Ca accompanied by many C elements, while the trace of Cl elements is dispersed in the particles.

Table 3. Elemental Analysis of Materials after Reaction[a]

elements	C	O	Al	Si	Cl	Ca	Ti
A	13.03	35.5	8.11	11.98	2.89	18.63	2.97
B	11.31	24.13	9.66	15.98	2.61	14.17	1.76
C	9.46	38.18	8.56	14.89	1.67	18.14	2.24
D	20.41	37.55	8.79	11.59	1.71	12.14	2.10
E	8.7	30.26	10.79	16.18	0.4	21.44	4.34
F	7.79	36.71	8.15	13.92	0.81	22.88	2.88

[a](wt/%).

https://doi.org/10.1021/acsomega.3c00612
ACS Omega 2023, 8, 19433−19442

4. CONCLUSIONS

This research was focused on the droplet interfacial behavior on heated extracted titanium tailing surfaces. The effects of surface temperature and Weber number on spreading characteristics were studied quantitatively. The mass fraction, elements, and microstructure of extracted titanium tailings after reaction were analyzed. The conclusions can be summarized below:

(1) The interfacial behaviors of the droplet impact on the extracted titanium tailings surface are classified into four regimes: boiling induced break-up, advancing recoiling, splash with a continuous liquid film, and splash with a broken film. In addition, when the droplet impacts on the extracted titanium tailing surface, no rebound phenomenon appears in the experiments. This is attributed to the capillary effects of the rough surface and the low thermal conductivity.

(2) Surface temperatures and Weber numbers have a critical influence on the droplet spreading factors. The surface temperatures and Weber numbers become larger, which leads to an increase in the maximum spreading factors. The scaling law of β_{max} is corrected as $\beta_{max} = 0.504We^{0.412}$.

(3) The Cl content of extracted titanium tailings before the dechlorination reaction is 5.08% by XRF analysis. When the surface temperature is raised to 500 °C, the weight loss ratio of the extracted titanium tailings after the reaction is reduced to 14%. Moreover, the Cl content is 1.03% from the results of the XRF analysis. The microstructure of extracted titanium tailings has some fine pores under the interfacial effect of droplet corrosion. The main compositions are Si, Al, and Ca oxides with a certain amount of C elements. The interfacial effect of liquid droplets on the extracted titanium tailings surface is enhanced, and the Cl content gradually decreases with the increased surface temperature. The interfacial effects of water droplets contribute significantly to accelerating the dechlorination reaction of the extracted titanium tailings.

AUTHOR INFORMATION

Corresponding Author

Liangying Wen − *School of Materials Science and Engineering, Chongqing University, Chongqing 400044, China; Chongqing Key Laboratory of Vanadium−Titanium Metallurgy and Advanced Materials, Chongqing University, Chongqing 400044, China;* orcid.org/0000-0002-7897-8952; Email: cquwen@cqu.edu.cn

Authors

Yan Zhao − *School of Materials Science and Engineering, Chongqing University, Chongqing 400044, China; Chongqing Key Laboratory of Vanadium−Titanium Metallurgy and Advanced Materials, Chongqing University, Chongqing 400044, China*

Bo Liu − *School of Materials Science and Engineering, Chongqing University, Chongqing 400044, China; Chongqing Key Laboratory of Vanadium−Titanium Metallurgy and Advanced Materials, Chongqing University, Chongqing 400044, China*

Li Su − *School of Materials Science and Engineering, Chongqing University, Chongqing 400044, China; Chongqing Key Laboratory of Vanadium−Titanium Metallurgy and Advanced Materials, Chongqing University, Chongqing 400044, China*

Meilong Hu − *School of Materials Science and Engineering, Chongqing University, Chongqing 400044, China; Chongqing Key Laboratory of Vanadium−Titanium Metallurgy and Advanced Materials, Chongqing University, Chongqing 400044, China;* orcid.org/0000-0002-5071-0700

Shengfu Zhang − *School of Materials Science and Engineering, Chongqing University, Chongqing 400044, China; Chongqing Key Laboratory of Vanadium−Titanium Metallurgy and Advanced Materials, Chongqing University, Chongqing 400044, China;* orcid.org/0000-0002-0858-7286

Jianxin Wang − *School of Materials Science and Engineering, Chongqing University, Chongqing 400044, China; Pangang Group Research Institute Co., Ltd., Panzhihua 617000, China*

Complete contact information is available at: https://pubs.acs.org/10.1021/acsomega.3c00612

Notes

The authors declare no competing financial interest.

ACKNOWLEDGMENTS

This work was supported by the National Natural Science Foundation of China (Grant no. 51974046).

REFERENCES

(1) Zheng, F.; Chen, F.; Guo, Y.; Jiang, T.; Travyanov, A. Y.; Qiu, G. Kinetics of hydrochloric acid leaching of titanium from titanium-bearing electric furnace slag. *JOM* **2016**, *68*, 1476−1484.

(2) Yang, J.; Tang, Y.; Yang, K.; Rouff, A. A.; Elzinga, E. J.; Huang, J. Leaching characteristics of vanadium in mine tailings and soils near a vanadium titanomagnetite mining site. *J. Hazard. Mater.* **2014**, *264*, 498−504.

(3) Zheng, F.; Guo, Y.; Qiu, G.; Chen, F.; Wang, S.; Sui, Y.; Jiang, T.; Yang, L. A novel process for preparation of titanium dioxide from Ti-bearing electric furnace slag: NH_4HF_2-HF leaching and hydrolyzing process. *J. Hazard. Mater.* **2018**, *344*, 490−498.

(4) Ma, H.; Jiao, K.; Zhang, J. The influence of basicity and TiO_2 on the crystallization behavior of high Ti-bearing slags. *CrystEngComm* **2020**, *22*, 361−370.

(5) Hou, X.; Wang, D.; Shi, Y.; Guo, H.; He, Y. Hydraulic activity and microstructure analysis of high-titanium slag. *Materials* **2020**, *13*, 1239.

(6) Chen, J.; Li, X.; Lu, Y.; Lin, L.; Wang, J.; Huang, S.; Yan, C.; Zhang, M.; Chen, H. Particle size controllable jet milling technology for efficiently recycling titanium-bearing blast furnace slag: numerical simulation and industrial test. *J. Clean. Prod.* **2020**, *247*, 119144.

(7) Zheng, F.; Li, M.; Wang, J.; Xi, C.; Fu, J.; Zhen, Q.; Jiao, Z.; Li, F.; Bashir, S.; Liu, J. Effective utilization of extracted titanium tailing to prepare high performance glass-ceramic and their formation mechanism. *Ceram. Int.* **2021**, *47*, 17391−17399.

(8) Landsberg, A.; Wilson, R. D.; Burns, W. Conditions affecting the formation of chlorinated carbon compounds during carbochlorination. *Metall. Mater. Trans. B* **1988**, *19*, 477−482.

(9) Valighazvini, F.; Rashchi, F.; Khayyam Nekouei, R. Recovery of titanium from blast furnace slag. *Ind. Eng. Chem. Res.* **2013**, *52*, 1723−1730.

(10) Andrade-Gamboa, J.; Pasquevich, D. M. A model for the role of carbon on carbochlorination of TiO_2. *Metall. Mater. Trans. B* **2000**, *31*, 1439−1446.

https://doi.org/10.1021/acsomega.3c00612
ACS Omega 2023, 8, 19433−19442

(11) Lin, S.; Qiushi, S.; Qian, X.; Zhiqiang, N.; Xionggang, L.; Derek, F. The electrochemical synthesis of TiC reinforced Fe based composite powder from titanium-rich slag. *New J. Chem.* **2015**, *39*, 4391−4397.
(12) Long, P. Z. Experimental researches on removal of Chloride in Blast Furnace slag after extracting titanium. *Gang Tie Fan Tai* **2014**, *35*, 42−45 (in Chinese).
(13) Ogata, F.; Tominaga, H.; Ueda, A.; Tanaka, Y.; Iwata, Y.; Kawasaki, N. Application of Activated Carbons from Coal and Coconut Shell for Removing Free Residual Chlorine. *J. Oleo Sci.* **2013**, *62*, 241−244.
(14) Guo, C. F.; Sun, Y. J.; Zhao, D. Y. Experimental study of droplet impact on superheated cylindrical surfaces. *Exp. Therm. Fluid Sci.* **2021**, *121*, 110263.
(15) Cossali, G. E.; Coghe, A.; Marengo, M. The impact of a single drop on a wetted solid surface. *Exp. Fluids* **1997**, *22*, 463−472.
(16) Avedisian, C. T.; Koplik, J. Leidenfrost boiling of methanol droplets on hot porous/ceramic surfaces. *Int. J. Heat Mass Transf.* **1987**, *30*, 379−393.
(17) Liang, G.; Mudawar, I. Review of drop impact on heated walls. *Int. J. Heat Mass Transf.* **2017**, *106*, 103−126.
(18) Castanet, G.; Liénart, T.; Lemoine, F. Dynamics and temperature of droplets impacting onto a heated wall. *Int. J. Heat Mass Transf.* **2009**, *52*, 670−679.
(19) Hamdan, K. S.; Kim, D. E.; Moon, S. K. Droplets behavior impactingon a hot surface above the Leidenfrost temperature. *Ann. Nucl. Energy* **2015**, *80*, 338−347.
(20) Bertola, V. An impact regime map for water drops impacting on heated surfaces. *Int. J. Heat Mass Transf.* **2015**, *85*, 430−437.
(21) Tran, T.; Staat, H. J. J.; Prosperetti, A.; Sun, C.; Lohse, D. Drop impact on superheated surfaces. *Phys. Rev. Lett.* **2012**, *108*, 036101.
(22) Jadidbonab, H.; Mitroglou, N.; Karathanassis, I.; Gavaises, M. Experimental study of diesel-fuel droplet impact on a similarly sized polished spherical heated solid particle. *Langmuir* **2018**, *34*, 36−49.
(23) Moita, A. S.; Moreira, A. L. N. Development of empirical correlations to predict the secondary droplet size of impacting droplets onto heated surfaces. *Exp. Fluids* **2009**, *47*, 755−768.
(24) Liang, G. T.; Guo, Y. L.; Yang, Y.; Guo, S.; Shen, S. Special phenomena from a single liquid drop impact on wetted cylindrical surfaces. *Exp. Therm. Fluid Sci.* **2013**, *51*, 18−27.
(25) Quéré, D. Leidenfrost Dynamics. *Annu. Rev. Fluid. Mech.* **2013**, *45*, 197−215.
(26) Bain, R. M.; Pulliam, C. J.; Thery, F.; Cooks, R. G. Accelerated chemical reactions and organic synthesis in Leidenfrost droplets. *Angew. Chem.* **2016**, *128*, 10634−10638.
(27) Abdelaziz, R.; Disci-Zayed, D.; Hedayati, M. K.; Pöhls, J.-H.; Zillohu, A. U.; Erkartal, B.; Chakravadhanula, V. S. K.; Duppel, V.; Kienle, L.; Elbahri, M. Green chemistry and nanofabrication in a levitated Leidenfrost drop. *Nat. Commun.* **2013**, *4*, 2400.
(28) Adda-Bedia, M.; Kumar, S.; Lechenault, F.; Moulinet, S.; Schillaci, M.; Vella, D. Inverse Leidenfrost Effect Levitating Drops on Liquid Nitrogen. *Langmuir* **2016**, *32*, 4179−4188.
(29) Zhao, Y.; Wen, L. Y.; Zhang, Y. F.; Liu, B.; Yang, H.; Deng, Q. Y. Experimental and Numerical Study on Dynamic Characteristics of Droplet Impacting on a Hot Tailings Surface. *Processes* **2022**, *10*, 1766.
(30) Zhao, Y.; Wen, L. Y.; Su, L.; Liu, B.; Wang, J. X.; Hu, L. W. Dynamics Behaviors of Droplets Impacting on a Heated Tailings Surface. 12th International Symposium on High-Temperature Metallurgical Processing. *12th International Symposium on High-Temperature Metallurgical Processing*; The Minerals, Metals & Materials Series, 2022; pp 185−196.
(31) Jin, Z. Y.; Sui, D. Y.; Yang, Z. G. The impact, freezing, and melting processes of a water droplet on an inclined cold surface. *Int. J. Heat Mass Transf.* **2015**, *90*, 439−453.
(32) Negeed, E. S. R.; Ishihara, N.; Tagashira, K.; Hidaka, S.; Kohno, M.; Takata, Y. Experimental study on the effect of surface conditions on evaporation of sprayed liquid droplet. *Int. J. Therm. Sci.* **2010**, *49*, 2250−2271.
(33) Harlow, F. H.; Shannon, J. P. The Splash of a Liquid Drop. *J. Appl. Phys.* **1967**, *38*, 3855−3866.
(34) Foltyn, P.; Ribeiro, D.; Silva, A.; Lamanna, G.; Weigand, B. Influence of wetting behavior on the morphology of droplet impacts onto dry smooth surfaces. *Phys. Fluids* **2021**, *33*, 063305.
(35) Zhao, P.; Hargrave, G. K.; Versteeg, H. K.; Garner, C. P.; Reid, B. A.; Long, E. J.; Zhao, H. The dynamics of droplet impact on a heated porous surface. *Chem. Eng. Sci.* **2018**, *190*, 232−247.
(36) Clanet, C.; Beguin, C.; Richard, D.; Quéré, D. Maximal deformation of an impacting drop. *J. Fluid Mech.* **2004**, *517*, 199−208.
(37) Wang, Z. F.; Xiong, J.; Yao, W.; Qu, W.; Yang, Y. Experimental investigation on the Leidenfrost Phenomenon of droplet impact on heated silicon carbide surfaces. *Int. J. Heat Mass Transf.* **2019**, *128*, 1206−1217.
(38) Liang, G. T.; Chen, Y.; Chen, L. Z.; Shen, S. Q. Maximum Spreading for Liquid Drop Impacting on Solid Surface. *Ind. Eng. Chem. Res.* **2019**, *58*, 10053−10063.
(39) Akao, F.; Araki, K.; Mori, S.; Moriyama, A. Deformation Behaviors of a Liquid Droplet Impinging onto Hot Metal Surface. *Trans. Iron Steel Inst. Jpn.* **1980**, *20*, 737−743.
(40) Joung, Y. S.; Buie, C. R. Scaling laws for drop impingement on porous films and papers. *Phys. Rev. E: Stat., Nonlinear, Soft Matter Phys.* **2014**, *89*, 013015.

https://doi.org/10.1021/acsomega.3c00612
ACS Omega 2023, 8, 19433−19442